Inorg. Chem. **2004**, *43*, 2859–2866

Synthesis and Oxygenation of a Nickel(II) and Zinc(II) Dithiolate: An Experimental and Theoretical Comparison

Craig A. Grapperhaus,* Christopher S. Mullins, Pawel M. Kozlowski, and Mark S. Mashuta

Department of Chemistry, University of Louisville, Louisville, Kentucky 40292

Received October 21, 2003

The diamino-dithiolato N_2S_2 ligand *N*,*N*′-bis-2-methyl-mercaptopropyl-*N*,*N*′-dimethylethylenediamine, H_2(bmmp-dmed), and its nickel (**1**) and zinc (**2**) complexes have been prepared and their reactivities with hydrogen peroxide investigated. Complex **1** yields a mixture of sulfenato (RSO^-), **4**, sulfinato (RSO_2^-), **3**, and sulfonato (RSO_3^-), **5**, products upon addition of H_2O_2. Products are separable by column chromatography. Stoichiometric addition of H_2O_2 to **2** yields an inseparable mixture. Excess peroxide addition results in oxygenation of the ligand to the disulfonate, **6**, and decomplexation of zinc. Complexes **1**, **2**, and **3** and compound **6** have been investigated by X-ray crystallography, and their structures are reported. Density functional theory (DFT) calculations of **1** and **2** reveal significant sulfur p character in the HOMO of each complex. However, **1** also shows significant metal d character that is π-antibonding with respect to the sulfur p orbitals. Complex **2** shows little metal character in the HOMO. Implications of the HOMO with respect to S-centered reactivity and metal ligand distances in S-oxygenated products are provided.

Introduction

The nucleophilicity of transition metal thiolates is well established, including reactivity toward oxygen and oxygen transfer agents to yield S-oxygenates.[1] One, two, or three oxygens may add per sulfur yielding sulfenato, sulfinato, or sulfonato complexes, respectively. To date, S-oxygenates of several metals have been prepared including, but not limited to, nickel,[1−7] cobalt,[8−20] iron,[14,15,16c,17] ruthenium,[21] and palladium.[22−24] Additionally, S-oxygenation of cysteine-112 and -114 at the iron or cobalt active site of nitrile hydratase is reportedly required for hydrolytic activity.[25−30] Studies of nickel S-oxygenates by Darensbourg[1,7] and others[3,4,6,7] reveal

* To whom correspondence should be addressed. E-mail: grapperhaus@louisville.edu. Phone: (502)852-5932. Fax: (502)852-8149.

(1) Grapperhaus, C. A.; Darensbourg, M. Y. *Acc. Chem. Res.* **1998**, *31*, 451−459.
(2) Farmer, P. J.; Solouki, T.; Mills, D. K.; Soma, T.; Russell, D. H.; Reibenspies, J. H.; Darensbourg, M. Y. *J. Am. Chem. Soc.* **1992**, *114*, 4601−4605.
(3) Kumar, M.; Colpas, G. J.; Day, R. O.; Maroney, M. J. *J. Am. Chem. Soc.* **1989**, *111*, 8323−8325.
(4) Maroney, M. J.; Choudhury, S. B.; Bryngelson, P. A.; Mirza, S. A.; Sherrod, M. J. *Inorg. Chem.* **1996**, *35*, 1073−1076.
(5) Schrauzer, G. N.; Zhang, C.; Chadha, R. *Inorg. Chem.* **1990**, *29*, 4104−4107.
(6) Henderson, R. K.; Bouwman, E.; Spek, A. L.; Reedijk, J. *Inorg. Chem.* **1997**, *36*, 4616−4617.
(7) Kaasjager, V. E.; Bouwman, E.; Gorter, S.; Reedijk, J.; Grapperhaus, C. A.; Reibenspies, J. H.; Smee, J. J.; Darensbourg, M. Y.; Derecskei-Kovacs, A.; Thomson, L. M. *Inorg. Chem.* **2002**, *41*, 1837−1844.
(8) Adzamli, I. K.; Deutsch, E. *Inorg. Chem.* **1980**, *19*, 1366−1373.
(9) Adzamli, I. K.; Libson, K.; Lydon, J. D.; Elder, R. C.; Deutsch, E. *Inorg. Chem.* **1979**, *18*, 303−311.
(10) Heinrich, L.; Li, Y.; Provost, K.; Michalowicz, A.; Vaissermann, J.; Chottard, J. C. *Inorg. Chim. Acta* **2001**, *318*, 117−126.
(11) Jackson, W. G.; Rahman, A. *Inorg. Chem.* **2003**, *42*, 383−388.
(12) Kung, I.; Schweitzer, D.; Shearer, J.; Taylor, W. D.; Jackson, H. L.; Lovell, S.; Kovacs, J. A. *J. Am. Chem. Soc.* **2000**, *122*, 8299−8300.
(13) Lydon, J. D.; Deutsch, E. *Inorg. Chem.* **1982**, *21*, 3180−3185.
(14) Mascharak, P. K. *Coord. Chem. Rev.* **2002**, *225*, 201−214.
(15) Noveron, J. C.; Olmstead, M. M.; Mascharak, P. K. *J. Am. Chem. Soc.* **2001**, *123*, 3247−3259.
(16) (a) Rat, M.; de Sousa, R. A.; Vaissermann, J.; Leduc, P.; Mansuy, D.; Artaud, I. *J. Inorg. Biochem.* **2001**, *84*, 207−213. (b) Rat, M.; de Sousa, R. A.; Tomas, A.; Frapart, Y.; Tuchaques, J. P.; Artaud, I. *Eur. J. Inorg. Chem.* **2003**, 759−765. (c) Galardon, E.; Giorgi, M.; Artaud, I. *Chem. Commun.* **2004**, 286−287.
(17) Tyler, L. A.; Noveron, J. C.; Olmstead, M. M.; Mascharak, P. K. *Inorg. Chem.* **1999**, *38*, 616−617.
(18) Tyler, L. A.; Noveron, J. C.; Olmstead, M. M.; Mascharak, P. K. *Inorg. Chem.* **2000**, *39*, 357−362.
(19) Tyler, L. A.; Noveron, J. C.; Olmstead, M. M.; Mascharak, P. K. *Inorg. Chem.* **2003**, *42*, 5751−5761.
(20) Tyler, L. A.; Olmstead, M. A.; Mascharak, P. K. *Inorg. Chem.* **2001**, *40*, 5408−5414.
(21) Dilworth, J. R.; Zheng, Y. F.; Lu, S. F.; Wu, Q. J. *Transition Met. Chem.* **1992**, *17*, 364−368.
(22) Grapperhaus, C. A.; Maguire, M. J.; Tuntulani, T.; Darensbourg, M. Y. *Inorg. Chem.* **1997**, *36*, 1860−1866.
(23) Tuntulani, T.; Musie, G.; Reibenspies, J. H.; Darensbourg, M. Y. *Inorg. Chem.* **1995**, *34*, 6279−6286.
(24) Cocker, T. M.; Bachman, R. E. *Inorg. Chem.* **2001**, *40*, 1550−1556.
(25) Endo, I.; Nojiri, M.; Tsujimura, M.; Nakasako, M.; Nagashima, S.; Yohda, M.; Odaka, M. *J. Inorg. Biochem.* **2001**, *83*, 247−253.
(26) Endo, I.; Odaka, M. *J Mol. Catal. B: Enzym.* **2000**, *10*, 81−86.
(27) Greene, S. N.; Chang, C. H.; Richards, N. G. J. *Chem. Commun.* **2002**, 2386-2387.
(28) Miyanaga, A.; Fushinobu, S.; Ito, K.; Wakagi, T. *Biochem. Biophys. Res. Commun.* **2001**, *288*, 1169−1174.

10.1021/ic035205y CCC: $27.50
Published on Web 03/26/2004

small structural changes compared to the thiolate precursors, with predictable electronic effects.[1,7] Similar observations have been more recently reported for iron and cobalt. Whereas S-oxygenation of several transition elements has been reported, such reactivity of zinc-thiolates has been largely unexplored.[31,32]

The biological roles of zinc-thiolates include N_2S_2-zinc finger proteins and cysteine-rich zinc alkylation proteins.[33−36] In the former, the metal serves a structural role and protects cysteine from disulfide formation. In the latter, the role of the zinc is to enhance the nucleophilicity of cysteine. In contrast to many transition elements, S-oxygenation has not been reported upon exposure of zinc-thiolates to oxygen. Studies by Wilcox *et al.* reveal that zinc "protects" the thiolate moiety upon exposure to hydrogen peroxide resulting in lessened formation of disulfide and thiolsulfinate.[31,32] It is intriguing that some metals enhance the reactivity of coordinated thiolates whereas others protect the thiolate from reactivity.

In this paper, we report the synthesis and oxygenation of nickel and zinc derivatives of the ligand *N*,*N*′-bis-2-methylmercaptopropyl-*N*,*N*′-dimethylethylenediamine, H_2(bmmpdmed). This provides a unique side by side comparison of two metals with different influences on sulfur reactivity: nickel (thiolate activation) and zinc (thiolate protection). The nickel derivative is closely related to a (N_2S_2)Ni complex previously reported by Reedijck and Darensbourg and displays similar reactivity.[6,7] While the focus of the previous study was S-oxygenation of nickel dithiolates with respect to S-oxygenate product distribution, this study is directed at the role of the metal. Experimental observations presented in the current paper are compared with theoretical investigations that reveal significant differences in the electronic structure of nickel and zinc dithiolates.

Experimental Section

Materials and Reagents. All chemicals were obtained from commercial sources and used as received unless otherwise noted. Isobutylene sulfide was prepared according to literature methods[37,38] and stored under N_2 at −20 °C. Reagent-grade solvents were dried using standard techniques and distilled under nitrogen prior to use. Deuterated solvents ($CDCl_3$, CD_3OD) were obtained from Cambridge Isotope Laboratories. Standard Schlenk techniques using nitrogen and a N_2-filled glovebox were used in synthesis of the complexes, although once obtained most of the pure products were stable in air.

Physical Methods. Elemental analyses were obtained from Midwest Microlab (Indianapolis, IN) or Galbraith Laboratories, Inc. (Knoxville, TN). IR spectra were recorded on a Thermo Nicolet Avatar 360 spectrometer at 4 cm^{-1} resolution. Electronic absorption spectra were recorded with an Agilent 8453 diode array spectrometer using 1 cm path length cells. NMR spectra were obtained on a Varian Inova500 500-MHz spectrometer. Cyclic voltammetric measurements were performed by using a PAR 273 potentiostat with a three-electrode cell (glassy carbon working electrode, platinum wire counter electrode, and Ag/AgCl reference electrode) at room temperature.

Crystallographic Studies. X-ray crystal structures were determined by Dr. Mark Mashuta at the X-ray diffraction laboratory in the chemistry department at the University of Louisville. Details of the data collection and refinement are displayed in Table 1.

A dark-purple 0.48 × 0.23 × 0.17 mm^3 crystal of **1** mounted on a glass fiber was used for X-ray crystallographic analysis. Data were collected at 293(3) K using the $\omega-2\theta$ scan technique on an Enraf-Nonius CAD4 diffractometer equipped with a Mo tube and a scintillation detector. A triclinic unit cell: $a = 6.162(2)$ Å, $b = 20.734(7)$ Å, $c = 12.334(7)$ Å, $\beta = 98.56(2)°$, $V = 1558(1)$ $Å^3$, $Z = 4$, and $\rho_{calcd} = 1.369$ Mg/m^3 yielded 2742 unique reflections, to a 2θ max = 50.00°, that were corrected for absorption (transmission min/max = 0.57/0.77; $\mu = 1.496$ mm^{-1}) using ψ-scans. The structure was solved by direct methods in the space group $P2_1/n$ using SHELXS-90[39] and refined by least-squares methods on F^2 using SHELXL-97[40] incorporated into the SHELXTL[41] (v 6.12) suite of programs. All non-hydrogen atoms were refined anisotropically. Hydrogen atoms were placed in their geometrically generated positions and refined as a riding model. Methylene Hs were included as fixed contributions with $U(H) = 1.2 \times U_{eq}$(attached C atom) while methyl groups were allowed to ride (the torsion angle which defines its orientation was allowed to refine) on the attached C atom, and these atoms were assigned $U(H) = 1.5 \times U_{eq}$. For all 2742 unique reflections (R(int) = 0.052), the final anisotropic full-matrix least-squares refinement on F^2 for 155 variables converged at R1 = 0.049 and wR2 = 0.129 with a GOF of 1.08.

A 0.23 × 0.14 × 0.06 mm^3 colorless single crystal of **2** was mounted on a 0.05 mm CryoLoop with Paratone oil for collection of X-ray data on a Bruker SMART APEX CCD diffractometer. The SMART[42] software package (v 5.625) was used to acquire a total of 1868 30-s frame ω-scan exposures of data at 100 K to a 2θ max = 54.78° using monochromated Mo Kα radiation (0.71073 Å) from a sealed tube and a monocapillary. Frame data were processed using SAINT[43] (v 6.22) to determine final unit cell parameters: $a = 7.083(3)$ Å, $b = 11.497(4)$ Å, $c = 20.830(7)$ Å, $V = 1696.3(10)$ $Å^3$ and to produce raw *hkl* data that were then corrected for absorption (transmission min/max = 0.75/0.90; $\mu = 1.678$ mm^{-1}) using SADABS[44] (v 2.02). The structure was solved

(29) Murakami, T.; Nojiri, M.; Nakayama, H.; Odaka, M.; Yohda, M.; Dohmae, N.; Takio, K.; Nagamune, T.; Endo, I. *Protein Sci.* **2000**, *9*, 1024−1030.
(30) Tsujimura, M.; Odaka, M.; Nakayama, H.; Dohmae, N.; Koshino, H.; Asami, T.; Hoshino, M.; Takio, K.; Yoshida, S.; Maeda, M.; Endo, I. *J. Am. Chem. Soc.* **2003**, *125*, 11532−11538.
(31) Xu, Y.; Wilcox, D. E. *J. Am. Chem. Soc.* **1998**, *120*, 7375−7376.
(32) Wilcox, D. E.; Schenk, A. D.; Feldman, B. M.; Xu, Y. *Antioxid. Redox Signaling* **2001**, *3*, 549−564.
(33) Demple, B.; Jacobsson, A.; Olsson, M.; Robins, P.; Lindahl, T. *J. Biol. Chem.* **1982**, *257*, 3776−3780.
(34) Myers, L. C.; Jackow, F.; Verdine, G. L. *J. Biol. Chem.* **1995**, *270*, 6664−6670.
(35) Myers, L. C.; Terranova, M. P.; Ferentz, A. E.; Wagner, G.; Verdine, G. L. *Science* **1993**, *261*, 1164−1167.
(36) Myers, L. C.; Terranova, M. P.; Nash, H. M.; Markus, M. A.; Verdine, G. L. *Biochemistry* **1992**, *31*, 4541−4547.
(37) Mills, D. K.; Font, I.; Farmer, P. J.; Hsiao, Y. M.; Tuntulani, T.; Buonomo, R. M.; Goodman, D. C.; Musie, G.; Grapperhaus, C. A.; Maguire, M. J.; Lai, C. H.; Hatley, M. L.; Smee, J. J.; Bellefeuille, J. A.; Darensbourg, M. Y. *Inorg. Synth.* **1998**, *32*, 89−98.
(38) Snyder, H. R.; Stewart, J. M.; Ziegler, J. B. *J. Am. Chem. Soc.* **1947**, *69*, 2672−2674.
(39) Sheldrick, G. M. SHELX-90. *Acta Crystallogr.* **1990**, *A46*, 467−473.
(40) Sheldrick, G. M. *SHELX-97. Program for the Refinement of Crystal Structures*; University Göttingen: Göttingen, Germany, 1997.
(41) *SHELXTL (v6.12), Program Library for Structure Solution and Molecular Graphics*; Bruker Advanced X-ray Solutions, Inc.: Madison, WI, 2001.
(42) *SMART*, v5.625; Bruker Advanced X-ray Solutions, Inc.: Madison, WI, 2001.
(43) *SAINT*, v6.22; Bruker Advanced X-ray Solutions, Inc.: Madison, WI, 2001.

Table 1. Crystal Data and Structure Refinement for **1**, **2**, **3**, and **6**

	1	**2**	**3**	**6**
empirical formula	$C_{12}H_{26}N_2S_2Ni$	$C_{12}H_{26}N_2S_2Zn$	$C_{12}H_{26}N_2S_2O_2Ni$	$C_{12}H_{28}N_2O_6S_2$
fw	321.18	327.84	353.18	360.48
temp (K)	293(2)	100(2)	293(2)	100(2)
wavelength (Å)	0.71073	0.71073	0.71073	0.71073
cryst syst	monoclinic	orthorhombic	monoclinic	monoclinic
space group	$P2_1/n$	*Pbcn*	$P2_1/n$	$P2_1/c$
unit cell dimens				
a (Å)	6.162(2)	7.083(3)	6.601(2)	11.5838(11)
b (Å)	20.734(7)	11.497(4)	12.502(4)	12.4871(12)
c (Å)	12.334(7)	20.830(7)	20.447(5)	12.0844(12)
β (deg)	98.56(3)		97.63(2)	98.660(2)
V (Å^3)	1558(1)	1696.3(10)	1677.8(6)	1728.1(3)
Z	4	4	4	4
d(calcd) (Mg/m^3)	1.369	1.284	1.398	1.386
abs coeff (mm^{-1})	1.496	1.678	1.405	0.336
cryst size (mm^3)	0.48 × 0.23 × 0.17	0.23 × 0.14 × 0.06	0.49 × 0.26 × 0.17	0.33 × 0.21 × 0.02
cryst color, habit	dark purple block	colorless plate	orange prism	colorless plate
θ range for data collection (deg)	2.58−25.00	1.96−27.39	2.01−27.5	1.78−28.12
index ranges	$-7 \le h \le 7$	$-8 \le h \le 8$	$-8 \le h \le 8$	$-16 \le h \le 16$
	$0 \le k \le 24$	$-14 \le k \le 14$	$0 \le k \le 16$	$-16 \le k \le 16$
	$0 \le l \le 14$	$-26 \le l \le 26$	$-26 \le l \le 26$	$-15 \le l \le 14$
reflns collected	2873	12545	7686	14837
indep reflns	2742	1830	3846	4007
	[R(int) = 0.0526]	[R(int) = 0.061]	[R(int) = 0.0376]	[R(int) = 0.045]
completeness to θ max	99.60%	95.00%	99.80%	95.20%
abs correction	ψ scans	SADABS	ψ scans	SADABS
min and max transm	0.57 and 0.77	0.753 and 0.904	0.73 and 0.83	0.893 and 0.992
refinement method	*c*	*c*	*c*	*c*
data/restraints/ params	2742/0/155	1830/0/81	3846/0/178	4007/0/312
GOF on F^2	1.088	1.017	1.008	1.039
final R indices	R1 = 0.048,	R1 = 0.043,	R1 = 0.039,	R1 = 0.037,
[$I > 2\sigma(I)$][a,b]	wR2 = 0.122	wR2 = 0.079	wR2 = 0.086	wR2 = 0.081
R indices (all data)[a,b]	R1 = 0.057,	R1 = 0.142,	R1 = 0.058,	R1 = 0.056,
	wR2 = 0.129	wR2 = 0.088	wR2 = 0.096	wR2 = 0.086
largest peak and hole (e·Å^{-3})	1.146 and −0.662	0.324 and −0.279	0.892 and −0.463	0.488 and −0.298

[a] $R1 = \sum||F_o| - |F_c||/\sum|F_o|$. [b] $wR2 = \{\sum[w(F_o^2 - F_c^2)^2]/\sum[w(F_o^2)^2]\}^{1/2}$; where $w = q/\sigma^2(F_o^2) + (qp)^2 + bp$. GOF = $S = \{\sum[w(F_o^2 - F_c^2)^2]/(n - p)\}^{1/2}$. [c] Full-matrix least-squares on F^2.

by direct methods and refined on F^2 using SHELXTL. All non-hydrogen atoms were refined anisotropically. Hydrogen atoms were placed in their geometrically generated positions and refined as a riding model as described above for **1**. For all 1830 unique reflections (R(int) = 0.061), the final anisotropic full-matrix least-squares refinement on F^2 for 81 variables converged at R1 = 0.043 and wR2 = 0.088 with a GOF of 1.01.

X-ray structural analysis for **3** was performed at 293(2) K on a 0.49 × 0.26 × 0.17 mm^3 orange prism using an identical data acquisition strategy described above for **1**. Compound **3** crystallizes in the monoclinic space group $P2_1/n$ with unit cell parameters a = 6.601(2) Å, b = 12.502(4) Å, c = 20.447(5) Å, β = 97.63(2)°, V = 1677.8(6) Å^3, Z = 4, and ρ_{calcd} = 1.398 Mg/m^3. There were 7686 total reflections collected to a 2θ max = 54.92° and corrected for absorption (transmission min/max = 0.57/0.77; μ = 1.496 mm^{-1}) using ψ-scans. The structure was solved by direct methods and refined on F^2 using SHELXTL. All non-hydrogen atoms were refined anisotropically. Hydrogen atoms were placed in their geometrically generated positions and refined as a riding model with fixed contributions described above for **1**. For all 3846 unique reflections (R(int) = 0.038), the final anisotropic full-matrix least-squares refinement on F^2 for 178 variables converged at R1 = 0.058 and wR2 = 0.096 with a GOF of 1.01.

X-ray structural analysis for **6** was performed on a 0.33 × 0.21 × 0.02 mm^3 colorless plate using an identical data acquisition strategy described above for **2** at 100 K to a 2θ max = 58.94°. Compound **6** crystallizes in the monoclinic space group $P2_1/c$ with unit cell parameters a = 11.5838(11) Å, b = 12.4871(12) Å, c = 12.0844(12) Å, β = 98.660(2)°, V = 1728.1(3) Å^3, Z = 4, and ρ_{calcd} = 1.386 Mg/m^3. There were 4007 raw independent reflections corrected for absorption (transmission min/max = 0.89/0.99; μ = 0.336 mm^{-1}) using SADABS[44] (v 2.02). The structure was solved by direct methods and refined on F^2 using SHELXTL. All non-hydrogen atoms were refined anisotropically. All hydrogen atoms were located by difference maps and refined isotropically. For all 4007 unique reflections (R(int) = 0.045), the final anisotropic full-matrix least-squares refinement on F^2 for 312 variables converged at R1 = 0.056 and wR2 = 0.086 with a GOF of 1.04. Additional details of the X-ray structural analysis for **1**, **2**, **3**, and **6** including atomic coordinates, anisotropic displacement parameters, as well as complete lists of bond lengths, angles, and torsion angles are available in CIF format in Supporting Information.

Syntheses. *N,N′*-Bis-2-methyl-mercaptopropyl-*N,N′*-dimethylethylenediamine, H_2(bmmp-dmed). Under anaerobic conditions, *N,N′*-dimethylethylenediamine (1.2 mL, 11 mmol) was added to a 50 mL Schlenk flask along with a 10-fold excess of isobutylene sulfide (12.0 mL, 122 mmol). The mixture was then stirred under a nitrogen atmosphere at 70 °C for 12−24 h. Upon cooling, the excess isobutylene sulfide was removed by vacuum evaporation yielding a colorless oil. ^{1}H NMR was performed to verify product formation. ^{1}H NMR ($CDCl_3$): δ 1.32 (s, 12 H), 1.44 (s, 2H), 2.41 (s, 4H), 2.49 (s, 4H), 2.70 (s, 6H). Yields are quantitative.

(44) Sheldrick, G. M. *SADABS (v2.02), Area Detector Absorption Correction*; University Göttingen: Göttingen, Germany, 1997.

(bmmp-dmed)Ni (1). A dry, degassed toluene solution (100 mL) of nickel acetylacetonate (13.8 g, 53.7 mmol) was added to a dry, degassed toluene solution (25 mL) of H_2(bmmp-dmed) (14.3 g, 54.0 mmol) in a 250 mL Schlenk flask. A purple solid precipitated immediately, and the mixture was stirred overnight at 22 °C. The mixture was filtered to obtain the crude product. The purple solid was washed with 2 × 50 mL portions of toluene and 2 × 100 mL portions of diethyl ether, and then allowed to air-dry (crude yield 11.9 g, 68.5%). Column chromatography (aluminum oxide, 0.4 m length) was employed using acetonitrile to elute a purple band that was found to be the pure product (7.95 g, 45.7%). Recrystallization from diethyl ether diffusion into a saturated methanol solution yielded X-ray quality crystals. Calcd (Found) for $NiC_{12}H_{26}N_2S_2$: C, 44.88 (44.99); H, 8.16 (8.32); N, 8.72 (8.65). NMR measurements were carried out in CD_3CN at room temperature. ^{1}H NMR: δ 1.3 (s, 6H), 1.46 (s, 6H), 2.18 (br, 1H), 2.39 (s, 2H), 2.55 (s, 2H), 2.81 (br, 1H), 3.08 (br, 6H). ^{13}C NMR: δ (ppm) 33.95, 37.18, 46.63, 60.20, 75.95.

(bmmp-dmed)Zn (2). Under anaerobic conditions, an ethanolic solution of H_2(bmmp-dmed) (2.85 g, 10.8 mmol) was added to a solution of NaH (2 equiv, 0.52 g, 22 mmol) in ethanol. The mixture was allowed to stir at room temperature for an hour, upon which an ethanolic solution of zinc chloride (1.47 g, 10.8 mmol) was slowly added via cannula to the deprotonated ligand, Na_2(bmmp-dmed). The cloudy mixture was then stirred for 48 h. The solvent was then removed under vacuum to give a white solid, which was washed first with water and then diethyl ether. Remaining sodium salts were removed by dissolution of the crude product into dichloromethane and extraction with water. Evaporation of the dichloromethane layer yielded a crude product that was washed with ether (1.06 g, 30%). X-ray quality crystals were obtained from evaporation of a saturated dichloromethane-diethyl ether solution. Calcd (Found) for $ZnC_{12}H_{26}N_2S_2$: C, 43.96 (43.78); H, 7.99 (7.66); N, 8.54 (8.33). NMR measurements were carried out in $CDCl_3$ at room temperature. ^{1}H NMR: δ 1.41 (s, 6 H), 1.45 (s, 6H), 2.41 (d, 2H), 2.50 (d, 2H), 2.61 (d, 2H), 2.63 (s, 6H), 2.86 (d, 2H). ^{13}C NMR: δ (ppm) 34.06, 37.23, 47.32, 56.87, 71.40.

(bmmp-O_2-dmed)Ni (3) and (bmmp-O-dmed)Ni (4). To a solution of **1** (1.00 g, 3.11 mmol) in CH_3OH (200 mL) at −78 °C was added 2 equiv (0.65 mL, 6.24 mmol) of H_2O_2 (30% aqueous) in CH_3OH (50 mL) dropwise with stirring over a 2 h period. The reaction mixture was allowed to slowly warm to room temperature and stirred for 24 h. After removal of solvent, the red-orange residue was then dissolved in acetonitrile and purified by chromatography on an alumina column. The following products were separated: the starting complex **1**, followed by a gold band, **3**, and an orange band, **4**. A small amount of green product (**5**) did not elute. Removal of solvent led to the isolation of a crude product with a yield ranging between 10% and 30% for complex **3**. Similar yields of **4** were obtained.

X-ray quality crystals of **3** were obtained by ether diffusion into a saturated MeCN solution. IR (KBr) ν (cm^{-1}): 1181, 1047 (S═O). Calcd (Found) for $NiC_{12}H_{26}N_2S_2O_2$: C, 40.81 (39.89); H, 7.42 (7.25); N, 7.93 (8.06). Attempts to isolate **4** in crystalline form were unsuccessful. IR(KBr) ν (cm^{-1}): 949 (S═O). Calcd (Found) for $NiC_{12}H_{26}N_2S_2O{\cdot}H_2O$: C, 40.58 (40.83); H, 7.95 (7.66); N, 7.89 (7.18).

(bmmp-O_6-dmed)Ni (5). A solution of **1** (105 mg, 0.33 mmol) in MeCN was cooled to −78 °C in a dry ice−acetone bath. H_2O_2 (30% aq , 6 equiv, 0.25 mL, 1.96 mmol) was added slowly, and the reaction mixture was stirred for 1 h and stored overnight at 4 °C. The mixture was anaerobically filtered to remove a small amount of lightly colored solid yielding a blue-green filtrate. The filtrate was reduced in volume to about 5 mL, and an equal volume of dry ether was added. The green precipitate thus obtained was filtered and washed with ether and vacuum-dried (37 mg, 25%). IR (KBr) ν (cm^{-1}): 1234, 1166, 1115, 1024 (S═O). Calcd (Found) for $NiC_{12}H_{26}N_2S_2O_6(H_2O)_2$: C, 31.80 (30.62); H, 6.67 (6.65); N, 6.18 (6.33).

Scheme 1

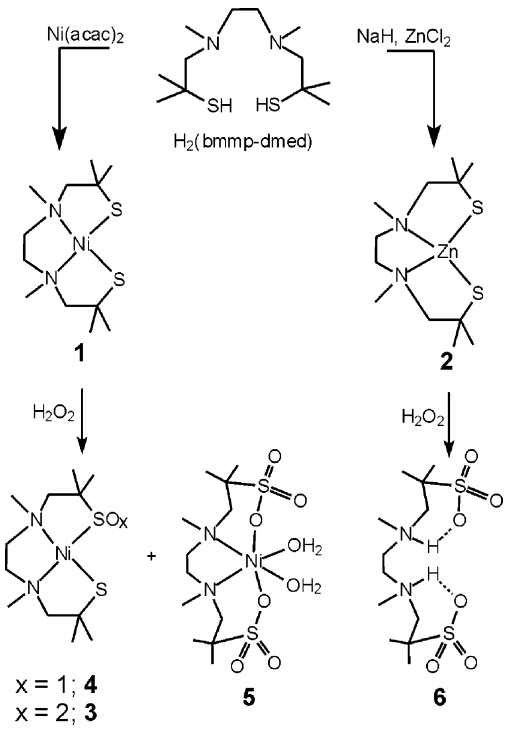

H_2(bmmp-O_6-dmed) (6). To a dichloromethane solution (25 mL) of **2** (180 mg, 0.55 mmol) was added 1.0 mL (9.7 mmol) of 30% H_2O_2. The reaction mixture was vigorously stirred for 48 h. A white precipitate was anaerobically filtered and then redissolved into water. The aqueous portion was then dried to give crude product. X-ray quality crystals were grown from slow evaporation of a saturated aqueous solution. However, due to the apparent decomposition of the product, satisfactory elemental analysis was not obtained. IR (KBr) ν (cm^{-1}): 3089 (N−H), 1232, 1166, 1114, 1024 (S═O). ESI-MS$^+$: *m*/*z* 361.

Results and Discussion

Synthesis and Characterization. The synthesis and reactivity of the nickel and zinc derivatives of the ligand, *N*,*N*′-bis-2-methyl-mercaptopropyl-*N*,*N*′-dimethylethylenediamine H_2(bmmp-dmed), are shown in Scheme 1. While H_2(bmmp-dmed) is in many ways similar to other N_2S_2 chelates previously reported, the presence of methyl substituents on the episulfide ring render the ethylene carbon relatively unreactive, preventing direct synthesis of H_2(bmmp-dmed) by standard methods.[37,45] Rather, addition of excess isobutylene sulfide in a neat reaction with the diamine results in quantitative conversion to the N_2S_2 chelate. The excess isobutylene sulfide is then removed under vacuum at room temperature yielding pure H_2(bmmp-dmed). A similar method was used previously in our laboratory for the synthesis of a related

(45) Grapperhaus, C. A.; Bellefeuille, J. A.; Reibenspies, J. H.; Darensbourg, M. Y. *Inorg. Chem.* **1999**, *38*, 3698−3703.

$N_2S_2S^*$ (S* = thioether) ligand.[46,47] Addition of H_2(bmmp-dmed) to Ni(acac)$_2$ in toluene yields the expected nickel complex, **1**, whereas the zinc derivative, **2**, can be prepared by addition of $ZnCl_2$ to Na_2(bmmp-dmed) in ethanol. The reaction of **1** with Cu(I) to make a bimetallic complex was previously reported.[48]

Both the nickel and zinc dithiolates **1** and **2** are stable to air in the solid state and in solution. Although the oxygen sensitivity of nickel thiolate complexes to yield nickel S-oxygenates is well established, it is also known that addition of methyl substituents on the α-carbon significantly reduces S-centered reactivity.[1,6,7] This is consistent with the behavior of **1** and **2**. Both **1** and **2** do, however, react with H_2O_2 to yield S-oxygenated products. As shown in Scheme 1, addition of stoichiometric quantities of H_2O_2 to **1** yield a red-orange mixture of products. Separation by alumina column chromatography allows recovery of unreacted **1** followed by a golden-brown band and an orange band. A light green band remains at the top of the column. Addition of excess quantities of H_2O_2 yields a green solution from which a homogeneous green precipitate is obtained.

From infrared analysis, the three oxygenated products can be assigned. The golden-brown product, **3**, displays intense bands at 1047 and 1182 cm^{-1}. This is similar to bands observed for previously reported Ni(SO_2R)(SR), nickel mono-sulfinato complexes.[1,6,7] The orange product, **4**, displays a peak at 949 cm^{-1} similar to bands observed for Ni(S(O)R)(SR), nickel mono-sulfenato complexes.[1] The green complex, **5**, displays several intense bands at 1234, 1166, 1115, and 1024 cm^{-1} suggesting its assignment as an O-bond disulfonate complex.[6,7] The UV−vis spectra of **3** and **4** are consistent with their assignments. Whereas **1** displays a visible band at 480 nm, attributed to a sulfur to metal charge transfer, this band is shifted in **3** and **4**. Complex **3** displays a band at 447 (580) nm nearly identical to the bands at 448 (270) nm reported for the closely related monosulfinato complex observed previously reported.[1] Complex **4** displays bands at 360 and 477 nm. The poor solubility of **5** prevented obtaining its UV−vis spectrum. However, the light green color of this product is indicative of nickel(II) in an octahedral environment and is qualitatively the same as the fully characterized nickel(II) disulfonato complex previously reported by Reedijk.[6,7] On the basis of IR and UV−vis characterization, the identities of the oxygenated products of **1** are assigned as monosulfenate (**3**), monosulfinate (**4**), and disulfonate (**5**). To our knowledge, this is the first example of the oxygenation of a coordinated thiolate to yield all three distinct oxygenation levels of sulfur in a single reaction.

Whereas the sulfur-oxygenation of nickel thiolates is well developed, less attention has been focused on the oxygenation of zinc thiolates. Addition of stoichiometric quantities (2 equiv) of H_2O_2 to **2** yields S-oxygenation, as determined by IR spectroscopy, although distinct products could not be isolated. Upon adding a large excess (17.6 equiv) of H_2O_2, a homogeneous product is obtained as a white precipitate, **6**. Following purification, this product displays bands in the IR, 1232, 1166, 1114, 1024 cm^{-1}, that are nearly identical to the disulfonato-nickel complex **5**. However, ESI-MS of **6** displays a major peak at $m/z = 361$ with an isotopic envelope consistent with $[H_3$(bmmp-dmed-$O_6)]^+$. Only a small peak assignable to a zinc-containing species at $m/z = 422.9$ is observed. Recrystallization of **6** yields pure, metal-free product (vida infra).

Table 2. Electrochemical Data from Cyclic Voltammetry in Acetonitrile for **1**, **3**, and **4**[a,b]

complex	E_{red}, V (ΔE_p, mV)	E_{ox},[c] V
1	−1.92 (106)	+0.41
3	−1.56 (137)	+0.77
4	−1.75 (103)	+0.48

[a] All potentials are measured at a scan rate of 200 mV/s at a glassy carbon electrode referenced to Ag/AgCl. [b] 2−5 mM solutions with 0.1 M TBAHFP as supporting electrolyte. [c] The process is irreversible. The potential recorded is E_{pc} (reductions) or E_{pa} (oxidations) measured at 200 mV/s.

Table 3. Selected Bond Distances (Å) and Bond Angles (deg) for **1**, **2**, and **3**

	1	**3**		**2**
Ni−S1	2.1479(10)	2.1339(9)	Zn−S1	2.237(1)
Ni−S2	2.1612(10)	2.1152(9)	Zn−N1	2.130(3)
Ni−N1	1.930(3)	1.945(2)	S1−Zn−S1′	144.24(7)
Ni−N2	1.950(3)	1.959(2)	N1−Zn−N1′	86.9(2)
S2−O1		1.468(3)		
S2−O2		1.470(3)		
S1−Ni−S2	95.16(4)	97.19(3)		
N1−Ni−N2	88.11(12)	89.06(10)		

Electrochemical Investigations. The electrochemical parameters of complexes **1**, **3**, and **4** are summarized in Table 2. The complexes display the expected behavior based on the work of Darensbourg.[1] Complex **1** displays a reversible event at −1.92 V that is assigned as $Ni^{II/I}$ reduction and an irreversible event at +0.41 V that is presumably ligand-centered.[1] Addition of a single oxygen atom, **4**, shifts the reduction potential positive by 170 mV consistent with the lessened donor ability of the sulfur upon addition of an electrophilic oxygen. Addition of a second oxygen to yield **3** further shifts the potentials by an additional +190 mV resulting in a reduction potential of −1.56 mV and an oxidation potential of +0.77 V.

X-ray Crystal Structure Analyses. The structures of complexes **1**−**3** as well as **6** have been determined by single-crystal X-ray techniques. Selected bond distances and angles for the nickel complexes **1** and **3** are provided in Table 3 with similar values for the zinc dithiolate, **2**.

Complex **1** crystallizes as dark purple blocks in the $P2_1/n$ space group from diethyl ether diffusion into a saturated methanol solution. A view of the molecular structure of **1** is shown in Figure 1. The bmmp-dmed ligand backbone adopts a pseudo-square-planar geometry about the central Ni atom. The donor environment is slightly twisted (14.1°) toward a tetrahedron. (The tetrahedral twist is defined as the angle of

(46) Grapperhaus, C. A.; Patra, A. K.; Mashuta, M. S. *Inorg. Chem.* **2002**, *41*, 1039−1041.
(47) Grapperhaus, C. A.; Li, M.; Patra, A. K.; Poturovic, S.; Kozlowski, P. M.; Zgierski, M. Z.; Mashuta, M. S. *Inorg. Chem.* **2003**, *42*, 4382−4388.
(48) Linck, R. C.; Spahn, C. W.; Rauchfuss, T. B.; Wilson, S. R. *J. Am. Chem. Soc.* **2003**, *125*, 8700−8701.

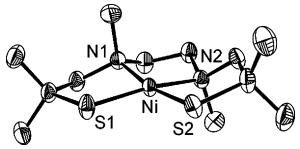

Figure 1. ORTEP view of **1** showing 50% probability displacement ellipsoids. H atoms are not shown.

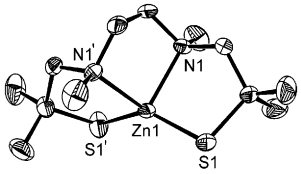

Figure 2. ORTEP view of **2** showing 50% probability displacement ellipsoids. H atoms are not shown.

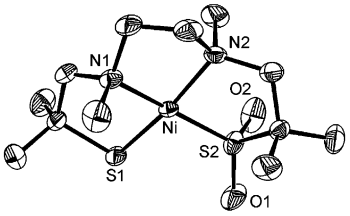

Figure 3. ORTEP view of **3** showing 50% probability displacement ellipsoids. H atoms are not shown.

intersection between a plane defined by N1, N2, and X1 and S1, S2, and X1 where X1 is the centroid of a plane defined by N1, N2, S1, and S2. For a square planar complex, this value is expected to be zero, whereas a tetrahedral complex would yield a value of 90°.)[1] The nickel sulfur bond distances of 2.1479(10) and 2.1612(10) Å are typical of square-planar, N_2S_2Ni diamino-dithiolato complexes. The nickel nitrogen distances of 1.930(3) and 1.950(3) Å are also standard. The N(1)−Ni−N(2) and N−Ni−S bond angles are slightly less than the ideal 90° while the S(1)−Ni−S(2) angle is obtuse, 95.16(4)°. The methyl groups on the nitrogen atoms are transoidal as in other ethylene bridged N_2S_2−Ni complexes.[6,7]

The zinc diamino-dithiolate, **2**, crystallizes as colorless plates in the orthorhombic space group *Pbcn* from dichloromethane/diethyl ether. A representation of the molecular structure of **2** is shown in Figure 2. The geometry about zinc is best described as distorted tetrahedral. Similar to **1**, the N(1)−Zn(1)−N(1′ bond angle is 86.9(2)° with N−Zn−S bond angles near 90°: N(1)−Zn(1)−S(1) = 91.42(9)°. Although these angles are apparently constrained by the five-membered rings resulting from coordination to Zn, the S(1)−Zn(1)−S(1′ angle, 144.24(7)°, has no such constraints. The tetrahedral twist angle for **2** is 72.4°. The Zn−S bond distances of 2.237(1) Å are slightly longer than the corresponding nickel complex. The Zn−N bond distances of 2.130(3) Å display a similar trend.

The monosulfinato complex **3** crystallizes in the $P2_1/n$ space group from acetonitrile. Figure 3 shows a representation of the molecular structure of **3**. The geometry about the nickel is pseudo-square-planar with a modest tetrahedral twist angle of 12.8°. The bond angles are similar to **1** with acute N−Ni−N and N−Ni−S bond angles, but an obtuse S(1)−Ni−S(2) bond angle, 97.19(3)°. Also, as in **1**, the

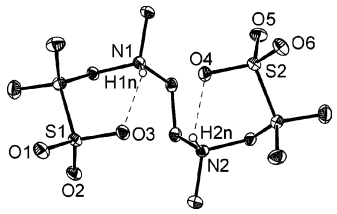

Figure 4. ORTEP view of **6** showing 50% probability displacement ellipsoids. Selected H atoms shown.

methyl groups on the nitrogens are transoidal. The Ni−S bond distance is insensitive to the oxygenation level of the sulfur: Ni−S(1), 2.1339(9) Å; Ni−S(2), 2.1152(9) Å (vida infra). The Ni−N(1) and Ni−N(2) bond distances of 1.945-(2) and 1.959(2) Å are largely unchanged from the thiolato precursor. The S(2)−O(1) and S(2)−O(2) bond distances are 1.468(3) and 1.470(3) Å.

Crystals of **6** isolated from the oxygenation of **2** are colorless plates in the $P2_1/c$ space group. The crystal structure clearly shows no coordinated metal atom as indicated by the ORTEP diagram illustrated in Figure 4. Compound **6** exists as a di-zwitterion with two protonated nitrogen atoms and two deprotonated sulfonic acid moieties. Although formally zwitterionic, the separation of charge is dissipated by the presence of two intramolecular hydrogen bonds. The H(1n) hydrogen is positioned between N(1) and O(3) with a N(1)−H(1n)−O(3) angle of 140.6° with a N(1)−H(1n) bond distance of 0.83(2) Å and a H(1n)···O(3) distance of 2.129 Å. H(2n) is similarly positioned between N(2) and O(4) with a N(2)−H(2n)−O(4) angle of 139.9° with a N(2)−H(2n) bond distance of 0.90(2) Å and a H(2n)···O(4) distance of 2.136 Å. As a result of the hydrogen bonding, **6** adopts a configuration much like the disulfonate ligand in (dsdm-O_6)-Ni.[6,7] Thus, the two H^+ ions sit in the metal-binding cavity of **6** in place of the anticipated metal, zinc. The S−O bond distances to the oxygens involved in H-bonding, 1.4120-(12) Å for S(1)−O(3) and 1.4365(13) Å for S(2)−O(4), are slightly shorter than the non-H-bonding S−O bond distances of 1.4922(13) Å for S(1)−O(1) and S(1)−O(2), 1.4590(13) Å for S(2)−O(6), and 1.4742(13) Å for S(2)−O(5).

Theoretical Investigations. Theoretical investigations of **1** and **2** were undertaken to further the understanding of the metal's influence on oxygenation reactions. To simplify computer effort, the methyl substituents on the carbons α to sulfur were omitted from **1** and **2**. The B3LYP exchange-correlation functional with the 6-31g(d) basis set was employed to optimize structures of the modified models, which are denoted **1*** and **2***. The Gaussian 98 suite of programs for electronic structure calculations was used to obtain full population analysis while Molekel was used for visualization.[49] A comparison of theoretical and experimental bond distances and angles is provided in Table S1. Overall, the experimental values are reproduced satisfactorily by the calculations. The slight overestimations in terms of bond lengths (0.02−0.05 Å) and bond angles (<4°) are within the accuracy of the B3LYP functional.

Figure 5 shows an orbital energy level diagram for complexes **1*** and **2***. The relative metal and sulfur contributions are provided in the Supporting Information. The results for

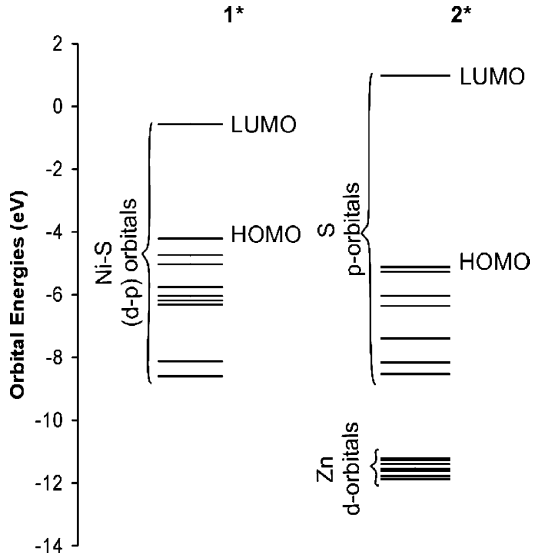

Figure 5. Energy level diagrams for **1*** and **2*** from DFT calculations.

1* are similar to those previously reported for a (N_2S_2)Ni complex by Darensbourg.[50] For complex **1***, the frontier region, LUMO to HOMO−8, contains orbitals with significant metal and sulfur character. For complex **2***, the orbitals are divided into a sulfur dominated region, LUMO to HOMO−6, and a zinc d-orbital region, HOMO−14 to HOMO−22. The lack of metal−sulfur interaction in **2** results from a mismatch in the energies of the zinc and sulfur orbitals and is not a result of symmetry, or geometry. This is consistent with the lower energy of zinc(II) d orbitals as compared to nickel(II).

The molecular orbital diagram of **1*** can be understood in simple terms by modifying the d orbital splitting pattern for a square-planar arrangement of σ-donor ligands to include two π-donors, Figure 6. Note the *z*-axis is assigned perpendicular to the metal−ligand plane, the *y*-axis bisects the S−Ni−S angle, and the *x*-axis bisects the N−Ni−S angle in accordance with DFT calculations. The p_z orbitals of sulfur are added as ligand group orbitals, either in-phase, denoted as LGO+, or out-of-phase, denoted as LGO− as shown in Figure 6. LGO− has the proper symmetry to overlap with the d_{xz} orbital in either an antibonding (HOMO) or bonding (HOMO−5) manner. Similarly, LGO+ combines with the d_{yz} orbital yielding HOMO−1 and HOMO−6. This results in the following molecular orbital assignments: LUMO (d_{xy}), HOMO (d_{xz} − LGO−), HOMO−1 (d_{yz} − LGO+), HOMO−2 (d_{z^2}), HOMO−3 ($d_{x^2-y^2}$), HOMO−4 (d_{yz} + LGO+), HOMO−5 (d_{xz} + LGO−). Although this view is admittedly simplified, it conveys a general representation of the key bonding features of the frontier orbitals and is consistent with the DFT calculations. For **2***, similar symmetry arguments could be made, but the difference in energy between the sulfur and zinc d-orbitals precludes overlap.

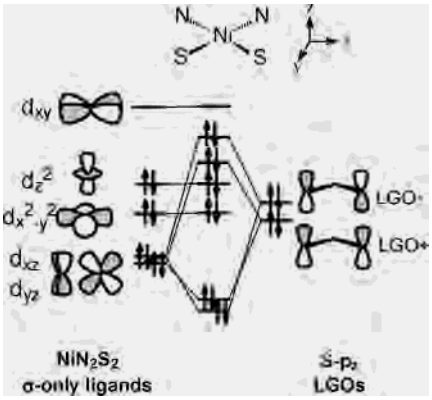

Figure 6. Qualitative molecular orbital diagram of the Ni−S, d−p π-bonding in **1**.

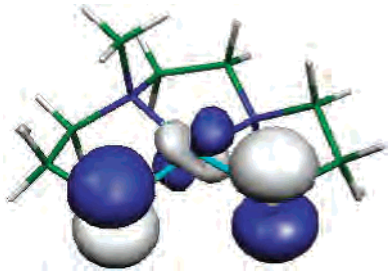

Figure 7. Representation of the HOMO of **1***.

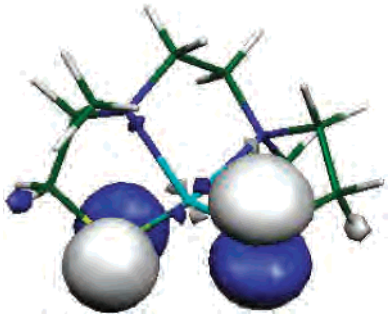

Figure 8. Representation of the HOMO of **2***.

Concluding Remarks

Insight into the reactivity of the nickel- and zinc-thiolates **1** and **2** can be ascertained from the structural models of the parent compounds, **1*** and **2***. Of particular interest is the nature of the HOMO, which contains the nucleophilic electron pair. Figures 7 and 8 show the HOMO orbital of **1*** and **2***, respectively. The HOMO of each complex shows significant sulfur p-character consistent with the observation that both **1** and **2** possess nucleophilic thiolates. The HOMO of **1*** and **2*** differ, however, in the metal's contribution. Understanding the role of the metal in the HOMO is key to

(49) Frisch, M. J.; Trucks, G. W.; Schlegel, H. B.; Scuseria, G. E.; Robb, M. A.; Cheeseman, J. R.; Zakrzewski, V. G.; Montgomery, J. A., Jr.; Stratmann, R. E.; Burant, J. C.; Dapprich, S.; Millam, J. M.; Daniels, A. D.; Kudin, K. N.; Strain, M. C.; Farkas, O.; Tomasi, J.; Barone, V.; Cossi, M.; Cammi, R.; Mennucci, B.; Pomelli, C.; Adamo, C.; Clifford, S.; Ochterski, J.; Petersson, G. A.; Ayala, P. Y.; Cui, Q.; Morokuma, K.; Malick, D. K.; Rabuck, A. D.; Raghavachari, K.; Foresman, J. B.; Cioslowski, J.; Ortiz, J. V.; Stefanov, B. B.; Liu, G.; Liashenko, A.; Piskorz, P.; Komaromi, I.; Gomperts, R.; Martin, R. L.; Fox, D. J.; Keith, T.; Al-Laham, M. A.; Peng, C. Y.; Nanayakkara, A.; Gonzalez, C.; Challacombe, M.; Gill, P. M. W.; Johnson, B. G.; Chen, W.; Wong, M. W.; Andres, J. L.; Head-Gordon, M.; Replogle, E. S.; Pople, J. A. *Gaussian 98*, revision A.11.4; Gaussian, Inc.: Pittsburgh, PA, 1998.

(50) Bellefeuille, J. A.; Grapperhaus, C. A.; Derecskei-Kovacs, A.; Reibenspies, J. H.; Darensbourg, M. Y. *Inorg. Chim. Acta* **2000**, *300*−*302*, 73−81.

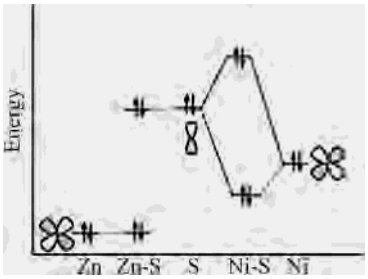

Figure 9. A simplified view of the π-interactions between a single sulfur p-orbital and a single metal d-orbital for zinc (left) and nickel (right).

understanding the metal's influence on the sulfur's nucleophilicity, since the electrons in the HOMO are a nucleophilic pair.

The HOMO of the nickel complex **1*** contains significant metal character that is π-antibonding with respect to the sulfur lone pairs, Figure 7. This has previously been referred to as a "π-repulsion" that increases the nucleophilicity of coordinated thiolates.[1,47,51] Another way to describe the effects of "π-repulsion" is to look at the effect of the metal on the energy of the thiolate lone pairs. Interactions that increase this energy will result in an enhanced thiolate nucleophilicity. As shown in Figure 6, the HOMO of **1*** is an antibonding combination of the filled metal d_{xy} orbital and the filled out-of-phase sulfur p-orbitals (LGO−). Figure 9 displays a simplified view of the π-bonding interaction between a single sulfur p-orbital and a single metal "t_{2g}" orbital. In the case of nickel, the energy of the metal-d and sulfur-p orbitals are comparable, resulting in significant overlap. Thus, the energy of the HOMO (the out-of-phase interaction) is significantly higher than that of the highest occupied atomic orbital (the sulfur p-orbital). This increase in energy enhances the nucleophilicity of the complex. As the HOMO is still largely sulfur-based, the presence of the nickel center increases the nucleophilicity of the coordinated thiolate.

The HOMO of the zinc-thiolate **2*** is localized essentially on the two sulfur atoms. The relatively low energy of the zinc d-orbitals precludes significant zinc-thiolate π-interactions (see Figure 9). The energy of the HOMO is not influenced by π-interactions with the zinc, and therefore, the nucleophilicity of the zinc-thiolates is not enhanced by the presence of the metal. This does not imply the zinc-thiolate is unreactive (the HOMO is still sulfur-p based), only that it should be less reactive than if a metal−sulfur interaction existed.

Additionally, the molecular orbital diagram is consistent with observed metal−sulfur bond distances in the reported complexes. For nickel and "t_{2g}" rich metals such as low-spin Fe, Co, and Ru, it has been observed that metal−sulfur bond distances in S-oxygenates are similar or even slightly shorter than that in the corresponding metal-thiolate.[1,47,51] The same trend is observed here, Table 3. This has been attributed to a combination of σ- and π-effects that result upon oxygenation of a coordinated thiolate. Upon oxygenation, the thiolate's lone pair(s) becomes involved in S−O bonding, eliminating the π-donor ability of the sulfur. As the π-interaction was antibonding, this should decrease the metal−sulfur bond distance. However, this effect is countered by a decreased σ-donor ability of sulfur-oxygenates relative to thiolates. This is equivalent to saying the ligand field strength of the $S_{oxgyenate}$ has increased relative to the $S_{thiolate}$ as the latter is a π-donor and the former is not. However, for zinc, complex **2**, there is no significant metal−sulfur π-interaction. Thus, oxygenation results only in a decrease in σ-donor ability and, hence, a measurable increase in Zn−S bond distance. In the case of **2**, the Zn−S bond dissociates. The same bond length effect, although Zn−SRR′ remains coordinated, is observed upon alkylation of nickel and zinc thiolates.[52]

In conclusion, a key difference between the nickel and zinc thiolates **1** and **2** is the presence of metal−sulfur π-interactions in the former, but not the latter. The metal−sulfur π-antibonding interaction enhances the nucleophilicity of the coordinated thiolate by raising energy of the sulfur lone pair. Additionally, the metal−sulfur π-antibonding interaction, and its loss upon oxygenation, is largely responsible for the similar $M-S_{thiolate}$ and $M-S_{oxygenate}$ bond distances for nickel. While the zinc thiolate **2** has the proper symmetry for a similar metal−sulfur π-interaction, the relatively low energy of the zinc d orbitals precludes significant overlap with the sulfur lone pair orbitals. Thus, the metal center does not enhance the nucleophilicity of the coordinated thiolate. Additionally, the absence of metal−sulfur π-interactions results in significant bond length increases, or even cleavage, upon oxygenation of zinc-thiolates. A combination of these nucleophilic and structural effects may partially explain the relatively large number of reported nickel S-oxygenates, but nonexistence of structurally characterized zinc S-oxygenates.

Acknowledgment is made to the donors of the Petroleum Research Fund, administered by the American Chemical Society, for partial support of this research (ACS PRF#37663-G3). Partial funding also provided by the National Science Foundation (CHE-0238137). C.S.M. thanks the Graduate School of the University of Louisville for a Research Fellowship. CCD X-ray equipment was purchased through funds provided by the Kentucky Research Challenge Trust Fund.

Supporting Information Available: X-ray structural data of **1**, **2**, **3**, and **6** in CIF format. Output log files from DFT calculations on **1*** and **2*** in txt format. Additional table. This material is available free of charge via the Internet at http://pubs.acs.org.

IC035205Y

(51) Ashby, M. T.; Enemark, J. H.; Lichtenberger, D. L. *Inorg. Chem.* **1988**, *27*, 191−197.

(52) Grapperhaus, C. A.; Mullins, C. S.; Kozlowski, P. K.; Mashuta, M. S. Manuscript in preparation.